Measurement of the mass and width of the $\Lambda_c(2625)^+$ charmed baryon and the branching ratios of $\Lambda_c(2625)^+ \to \Sigma_c^0 \pi^+$ and $\Lambda_c(2625)^+ \to \Sigma_c^{++}\pi^-$

D. Wang, J. Yelton, I. Adachi, J. K. Ahn, H. Aihara, D. M. Asner, H. Atmacan, R. Ayad, V. Babu,
Sw. Banerjee, M. Bauer, P. Behera, K. Belous, J. Bennett, M. Bessner, T. Bilka, D. Biswas, D. Bodrov,
J. Borah, A. Bozek, M. Bračko, P. Branchini, T. E. Browder, A. Budano, M. Campajola, D. Červenkov,
M.-C. Chang, A. Chen, B. G. Cheon, H. E. Cho, K. Cho, S.-J. Cho, S.-K. Choi, Y. Choi, S. Choudhury,
D. Cinabro, S. Das, G. De Nardo, G. De Pietro, R. Dhamija, F. Di Capua, Z. Doležal, T. V. Dong,
D. Dossett, D. Epifanov, T. Ferber, D. Ferlewicz, B. G. Fulsom, R. Garg, V. Gaur, A. Giri, P. Goldenzweig,
E. Graziani, T. Gu, K. Gudkova, C. Hadjivasiliou, X. Han, K. Hayasaka, H. Hayashii, M. T. Hedges,
C.-L. Hsu, K. Inami, N. Ipsita, A. Ishikawa, R. Itoh, M. Iwasaki, W. W. Jacobs, E.-J. Jang, S. Jia, Y. Jin,
A. B. Kaliyar, K. H. Kang, T. Kawasaki, C. Kiesling, C. H. Kim, D. Y. Kim, K.-H. Kim, Y.-K. Kim,
K. Kinoshita, P. Kodyš, A. Korobov, S. Korpar, E. Kovalenko, P. Križan, P. Krokovny, M. Kumar,
R. Kumar, K. Kumara, Y.-J. Kwon, T. Lam, J. S. Lange, S. C. Lee, D. Levit, P. Lewis, L. K. Li, Y. Li,
Y. B. Li, L. Li Gioi, J. Libby, K. Lieret, Y.-R. Lin, D. Liventsev, T. Matsuda, D. Matvienko, F. Meier,
M. Merola, F. Metzner, K. Miyabayashi, R. Mizuk, G. B. Mohanty, R. Mussa, I. Nakamura, T. Nakano,
M. Nakao, Z. Natkaniec, A. Natochii, L. Nayak, M. Nayak, N. K. Nisar, S. Nishida, S. Ogawa, H. Ono,
P. Oskin, G. Pakhlova, S. Pardi, H. Park, J. Park, S. Patra, S. Paul, T. K. Pedlar, R. Pestotnik,
L. E. Piilonen, T. Podobnik, E. Prencipe, M. T. Prim, N. Rout, G. Russo, S. Sandilya, A. Sangal, L. Santelj,
V. Savinov, G. Schnell, J. Schueler, C. Schwanda, Y. Seino, K. Senyo, M. E. Sevior, W. Shan, M. Shapkin,
C. Sharma, C. P. Shen, J.-G. Shiu, A. Sokolov, E. Solovieva, M. Starič, M. Sumihama, T. Sumiyoshi,
W. Sutcliffe, M. Takizawa, U. Tamponi, K. Tanida, F. Tenchini, M. Uchida, S. Uno, R. van Tonder,
G. Varner, K. E. Varvell, A. Vinokurova, M.-Z. Wang, X. L. Wang, M. Watanabe, S. Watanuki,
O. Werbycka, E. Won, X. Xu, B. D. Yabsley, W. Yan, S. B. Yang, J. H. Yin, C. Z. Yuan,
L. Yuan, Z. P. Zhang, V. Zhilich, and V. Zhukova

(Belle Collaboration)

Using the entire data sample of 980 fb^{-1} collected at or near the $\Upsilon(4S)$ resonance with the Belle detector operating at the KEKB asymmetric-energy e^+e^- collider, we report the measurement of the mass, width, and the branching ratios of the $\Lambda_c(2625)^+$ charmed baryon. The mass difference between $\Lambda_c(2625)^+$ and Λ_c^+ is measured to be $M(\Lambda_c(2625)^+) - M(\Lambda_c^+) = 341.518 \pm 0.006 \pm 0.049$ MeV/c^2. The upper limit on the width is measured to be $\Gamma(\Lambda_c(2625)^+) < 0.52$ MeV/c^2 at 90% confidence level. Based on a full Dalitz plot fit, branching ratios with respect to the mode $\Lambda_c(2625)^+ \to \Lambda_c^+ \pi^+ \pi^-$ are measured to be $\frac{\mathcal{B}(\Lambda_c(2625)^+ \to \Sigma_c^0 \pi^+)}{\mathcal{B}(\Lambda_c(2625)^+ \to \Lambda_c^+ \pi^+ \pi^-)} = (5.19 \pm 0.23 \pm 0.40)\%$ and $\frac{\mathcal{B}(\Lambda_c(2625)^+ \to \Sigma_c^{++} \pi^-)}{\mathcal{B}(\Lambda_c(2625)^+ \to \Lambda_c^+ \pi^+ \pi^-)} = (5.13 \pm 0.26 \pm 0.32)\%$, where the first and second uncertainties are statistical and systematic, respectively. These measurements can be used to further constrain the parameters of the underlying theoretical models.

I. INTRODUCTION

The Λ_c^+ charmed baryons consist of a heavy charm quark and two light (ud) quarks with the ground state having quantum numbers $J^P = \frac{1}{2}^+$. The $\Lambda_c(2595)^+$ and $\Lambda_c(2625)^+$ are the two lowest-lying excited states observed and are generally believed to have $J^P = \frac{1}{2}^-$ and $J^P = \frac{3}{2}^-$, respectively. The $\Lambda_c(2595)^+$ predominantly decays to the $J^P = \frac{1}{2}^+$ $\Sigma_c(2455)^{++/0}$ states via an s-wave decay. The analogous decay for the $\Lambda_c(2625)^+$ to the $J^P = \frac{3}{2}^+$ $\Sigma_c(2520)^{++/0}$ states is kinematically suppressed as it can only happen through the low-mass tail of the $\Sigma_c(2520)^{++/0}$. The d-wave decay to the $J^P = \frac{1}{2}^+$ $\Sigma_c(2455)^{++/0}$ states is allowed, but its

contribution is known to be small. Thus, the $\Lambda_c(2625)^+$ decay is thought to proceed primarily via the direct three-body, p-wave decay $\Lambda_c(2625)^+ \to \Lambda_c^+ \pi^+ \pi^-$.

The $\Lambda_c(2625)^+$ was first observed in 1993 [1]. The CDF Collaboration reported the most recent measurements of $\Lambda_c(2625)^+$ properties in 2011 using a data sample of 6.2×10^3 events [2]. Their measurement for the $\Lambda_c(2625)^+$ mass with respect to the Λ_c^+ mass is much more precise compared with previous measurements, and an upper limit on the $\Lambda_c(2625)^+$ width was reported. The limited decay phase space of $\Lambda_c(2625)^+ \to \Lambda_c^+ \pi^+ \pi^-$ makes it difficult to extract the $\Sigma_c(2455)^{++/0}$ yields by fitting the $\Lambda_c^+ \pi^\pm$ invariant mass due to the presence of reflection peaks formed by the combination of the Λ_c^+ and the other final-state pion. The large data sample collected by Belle, together with the use of an amplitude model [3] to describe the decay, allows us to use a full Dalitz fit that naturally includes the reflections.

The mass of the $\Lambda_c(2625)^+$, relative to the Λ_c^+ mass, is already relatively well known, but the large Belle data sample allows for a more precise measurement. No intrinsic width of the $\Lambda_c(2625)^+$ has yet been measured, and the current upper limit $\Gamma < 0.97$ MeV/c^2 at 90% confidence level by the Particle Data Group (PDG) [4] is based on the CDF measurement.

Theoretical predictions for the width vary for this narrow state [3,5–7]. An improved limit on the width of the $\Lambda_c(2625)^+$ will help to constrain these predictions and provide insights into other charmed baryons since their widths are related through common coupling constants [8].

II. DETECTOR AND DATASET

The measurement presented here is based on the entire dataset collected by the Belle detector [9,10] operating at the KEKB asymmetric-energy e^+e^- collider [11,12]. The total integrated luminosity of the dataset is 980 fb^{-1}, which is mostly collected at or near the $\Upsilon(4S)$ resonance.

The Belle detector is a large-solid-angle magnetic spectrometer that consists of a silicon vertex detector (SVD), a 50-layer central drift chamber (CDC), an array of aerogel threshold Cherenkov counters (ACCs), a barrel-like arrangement of time-of-flight scintillation counters (TOF), and an electromagnetic calorimeter composed of CsI(Tl) crystals (ECL) located inside a superconducting solenoid coil that provides a 1.5 T magnetic field. An iron flux-return locatedæ outside of the coil is instrumented to detect K_L^0 mesons and to identify muons. The detector is described in detail elsewhere [9]. Two inner detector configurations were used. The first consisted of a 2.0 cm radius beam pipe and a three-layer silicon vertex detector, while the second used a 1.5 cm radius beam pipe, a four-layer silicon detector, and a small-cell inner drift chamber.

Monte Carlo (MC) events are generated using EvtGen [13] to optimize selection criteria and to be used in the Dalitz plot fit. The $\Lambda_c(2625)^+ \to \Lambda_c^+ \pi^+ \pi^-$ and $\Lambda_c^+ \to pK^-\pi^+$ samples are generated using a phase space model [14]. A $D^{*+} \to D^0\pi^+$, with $D^0 \to K^-\pi^+$, sample is also generated to compare the mass-resolution function in the MC sample and the experimental data, and thus to estimate the systematic uncertainties on the measurements. The detector response is simulated with GEANT3 [15] and the event reconstruction is performed using data converted with the Belle-to-Belle-II (B2BII) software package [16] and then analyzed using BELLE II software [17,18].

III. ANALYSIS

The candidate $\Lambda_c(2625)^+$ baryons are reconstructed from the decay chain $\Lambda_c(2625)^+ \to \Lambda_c^+ \pi^+ \pi^-$, $\Lambda_c^+ \to pK^-\pi^+$. The final-state charged particles, $\pi^\pm$, K^-, and p, are selected based on the likelihood information from the tracking (SVD, CDC) and particle identification (CDC, ACCs, TOF) systems into a combined likelihood, $\mathcal{L}(h_1:h_2) = \mathcal{L}(h_1)/(\mathcal{L}(h_1) + \mathcal{L}(h_2))$, where h_1 and h_2 are p, K, or π [19]. We require the proton candidates to have $\mathcal{L}(p:K) > 0.6$ and $\mathcal{L}(p:\pi) > 0.6$, kaon candidates to have $\mathcal{L}(K:p) > 0.6$ and $\mathcal{L}(K:\pi) > 0.6$, and pion candidates to have $\mathcal{L}(\pi:K) > 0.6$ and $\mathcal{L}(\pi:p) > 0.6$. Electrons are suppressed by requiring $\mathcal{L}(e^-)/(\mathcal{L}(e^-) + \mathcal{L}(\text{hadrons})) < 0.1$ for all candidates; the likelihoods $\mathcal{L}(e^-)$ and $\mathcal{L}(\text{hadrons})$ include information from the ECL in addition to the tracking and particle identification systems [19]. The particle identification efficiency is approximately 87% for protons, 85% for kaons, and 96% for pions. Charged tracks are also required to have a point of closest approach with respect to the interaction point less than 3 cm in the e^+ beam direction and less than 1 cm in the plane perpendicular to it.

A vertex fit is applied to the daughter particles of the Λ_c^+ candidates and the resultant χ^2 probability of the fit is required to be greater than 0.001. Candidates within ± 7.0 MeV/$c^2 (\approx 1.6\sigma)$ are selected and mass constrained to the Λ_c^+ PDG mass of 2286.46 MeV/c^2 [4]. Two pions of opposite charge are then combined with the constrained Λ_c^+ candidate to form a $\Lambda_c(2625)^+$ candidate. The $\Lambda_c(2625)^+$ daughters are then kinematically fitted to come from a common vertex, with a constraint that the vertex has to be within the beam spot since the $\Lambda_c(2625)^+$ is short-lived. The χ^2 probability of this fit is required to be greater than 0.001 to ensure the quality of the fit. As excited charmed baryons including the $\Lambda_c(2625)^+$ typically have a hard momentum distribution, we only keep $\Lambda_c(2625)^+$ candidates with $x_p > 0.7$, where $x_p = p^*/\sqrt{E_{\text{beam}}^2/c^2 - M^2c^2}$ and p^* is momentum of the $\Lambda_c(2625)^+$ in the e^+e^- center of mass frame. As the mass of the Λ_c^+ is constrained to its PDG value, the reconstructed mass $M(\Lambda_c^+\pi^+\pi^-)$ has the resolution of the mass difference $M(\Lambda_c(2625)^+) - M(\Lambda_c^+)$.

Correctly calibrating the momentum scale for low-momentum pions is critical for this analysis. We calibrate

the momentum scale using copious $K_S^0 \to \pi^+\pi^-$ events in the experimental data. Low-momentum tracks are iteratively calibrated as a function of the polar angle and momentum of each track in the laboratory frame by comparing the reconstructed and world-average mass of the K_S^0 meson as a function of the K_S^0 momentum. This correction has been used in a previous $\Sigma_c^{++/0}$ study using Belle data [20]. Since the mass-resolution function is crucial for the precise measurement of the $\Lambda_c(2625)^+$ mass and width, the MC sample tracks are smeared using the analysis software during reconstruction, as otherwise the MC sample mass resolution is known to be better than that of the experimental data. This track smearing affects the width of the mass-resolution function but not its central value. The mass-resolution function of the $\Lambda_c(2625)^+$ mass is parametrized as a sum of two Gaussian functions with parameters fixed according to a signal MC sample with both corrections as detailed above.

The consistency between the MC sample and the experimental data is checked by comparing the mass resolution of D^{*+} events, which have similar kinematics to the events under study. The low-momentum track correction ensures that the measured D^{*+} mass in data and MC sample are independent of the momentum of the soft pion [20]. The resolution of the D^{*+} mass relative to the D^0 mass in the experimental data is found by fitting the $M(D^0\pi^+) - M(D^0)$ mass distribution in the experimental data with a Breit-Wigner distribution convolved with a double-Gaussian mass-resolution function, where the width of the Breit-Wigner distribution is fixed to the PDG value of 83.4 keV/c^2 [4]. In this study, without track smearing, the mass resolution in the experimental data is measured to be 114% of the value obtained from the MC sample. However, with track smearing, the mass resolution in the experimental data is measured to be 86% of the value obtained from the MC sample. In all other narrow signals studied, for instance the Λ_c^+, the track smearing ensures that the MC sample and data agree reasonably. The track smearing has negligible effect on the mass measurement. The results of these consistency checks are used in the estimation of the systematic uncertainties described below.

The reconstructed $M(\Lambda_c^+\pi^+\pi^-)$ mass distribution in the experimental data is fitted using RooFit [21]. Figure 1 shows the $M(\Lambda_c^+\pi^+\pi^-)$ mass distribution in the experimental data overlaid with the fit result. The signal function is a Breit-Wigner distribution convolved with a double-Gaussian mass-resolution function, and the background function is a second-order Chebyshev polynomial. The resolution function for the invariant mass distribution is obtained from the MC sample, without track smearing, and scaled by 114% in accordance with the D^{*+} study. The solid line shows the overall fit and the dashed lines show the individual signal and background components of the fit. The fitted mass is 2628.025 $\pm$ 0.006 MeV/c^2, independent of which version of the mass-resolution function we use.
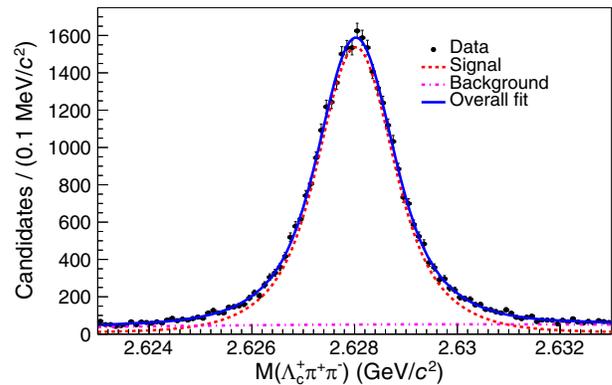
FIG. 1. Distribution of the invariant mass $M(\Lambda_c^+\pi^+\pi^-)$ where the Λ_c^+ mass is fixed to the PDG value. The solid line shows the overall distribution and the dashed lines show the individual signal and background components.

The uncertainty is statistical only. If we use the track-smearing correction without any rescaling, the fitted width is found to be zero, so we have no definitive evidence of a nonzero width and will present only an upper limit for the measurement of the intrinsic width of the $\Lambda_c^+(2625)$. If we scale by 114% the mass-resolution function without track smearing, the fitted width is 0.490 $\pm$ 0.025 MeV/c^2. If we scale by 86% the mass-resolution function with track smearing, the fitted width is 0.293 $\pm$ 0.026 MeV/c^2. These finite values for the fitted width after scaling the mass resolution are only used to find the limit on the intrinsic width including systematic uncertainties.

The fitted mass of $\Lambda_c(2625)^+$ in the signal MC sample is slightly different from the generated value. Applying a bias correction, determined by the mass shift observed in the signal MC sample, the mass of the $\Lambda_c(2625)^+$ is measured to be 2627.978 $\pm$ 0.006 MeV/c^2, where the uncertainty is statistical.

Two upper limits on the width are calculated based on the two mass-resolution functions methods described above and the larger upper limit is reported as the final answer. Using the mass-resolution function determined from MC sample scaled by 114% without track smearing, the upper limit is determined to be

$$\Gamma(\Lambda_c(2625)^+) < 0.52 \text{ MeV}/c^2 \qquad (1)$$

at 90% confidence level by integrating the likelihood function to find the value for which the integral contains 90% of the total area. Using the mass-resolution function scaled by 86% with track smearing would yield a tighter upper limit. Therefore, we conservatively report the former as the upper limit on the width of $\Lambda_c(2625)^+$.

IV. DALITZ PLOT FIT

A Dalitz plot fit is made in order to determine the branching ratios of $\Lambda_c(2625)^+$ with respect to the mode
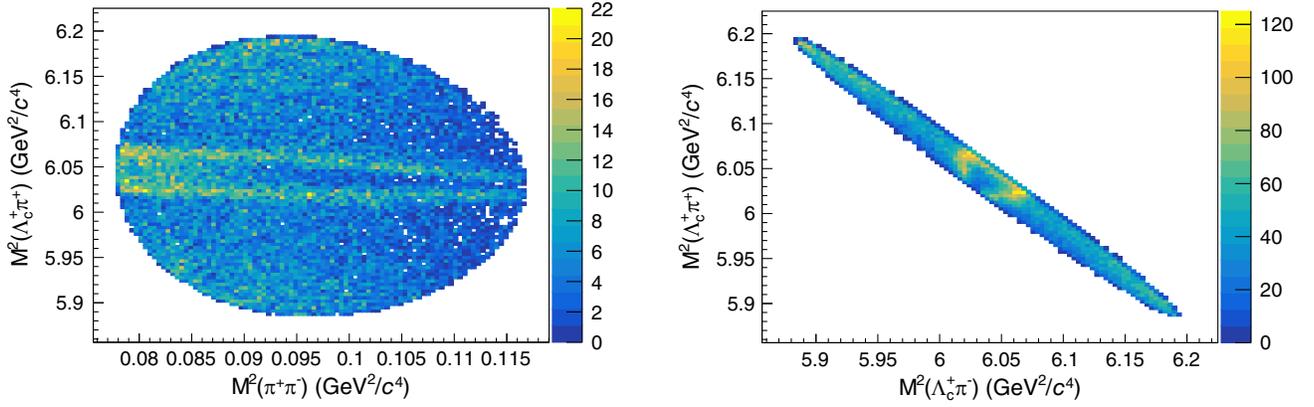
FIG. 2. Dalitz plot for $\Lambda_c(2625)^+$ candidates in the signal region. Explanations of the patterns in the text.

$\Lambda_c(2625)^+ \to \Lambda_c^+\pi^+\pi^-$. For the Dalitz plot fit, only $\Lambda_c(2625)^+$ candidates within ± 2 MeV/c^2 of the $\Lambda_c(2625)^+$ PDG mass are accepted [4]. The invariant mass of the $\Lambda_c(2625)^+$ candidates is then constrained to the $\Lambda_c(2625)^+$ PDG mass of 2628.11 MeV/c^2, and the four-vectors of the daughter particles are updated accordingly. A fit is made to the Dalitz plot using an amplitude model as presented by Arifi *et al.* [3] using the AmpTools software package [22]. The $\Lambda_c(2625)^+$ signal distribution is calculated from the squared amplitude with spin sum of final states and spin average of the initial states

$$\sum |\mathcal{T}_1 + \mathcal{T}_2 + \mathcal{T}_3 + \mathcal{T}_4 + \mathcal{T}_5|^2, \qquad (2)$$

where $\mathcal{T}_1$–$\mathcal{T}_5$ are the decay amplitudes through the intermediate states Σ_c^0, $\Sigma_c(2520)^0$, Σ_c^{++}, $\Sigma_c(2520)^{++}$, and the direct three-body decay, respectively. Each amplitude is modeled as a Breit-Wigner distribution function multiplied by a form factor specific to each decay channel. A constant amplitude is used to model the background $\Lambda_c^+\pi^+\pi^-$ combinations, which are not decay products of $\Lambda_c(2625)^+$. The yield of each decay channel is calculated using AmpTools by an integration of the individual component over the Dalitz plot. The contribution of the three-body decay in the signal model is different from the background phase space decay in that the former is not flat across the Dalitz plot. During the fit, the masses and widths of these intermediate particles are constrained to their respective PDG values to facilitate the convergence. The small variations of the detector acceptance across the Dalitz plot are taken into account by using the output of a phase space MC sample passed through the GEANT3 detector simulation as input to the AmpTools fitting package.

Figure 2 shows the Dalitz plots for candidates in the signal region. On the left panel, the contributions from Σ_c^{++} and the reflection from Σ_c^0 constitute the two horizontal stripes. The upper and lower parts of the Dalitz plot show slight excesses due to $\Sigma_c(2520)^{++/0}$ decays. There is also a clear excess on the left side of the Dalitz plot compared to the right in agreement with the three-body decay taking into account the spin, as predicted in the amplitude model [3]. On the right panel, the horizontal and vertical stripes indicate the Σ_c^{++} and Σ_c^0 decays, respectively. It is straightforward to see the origin of the reflection peaks on the $M(\Lambda_c^+\pi^+)$ mass projection from this 2D Dalitz plot.
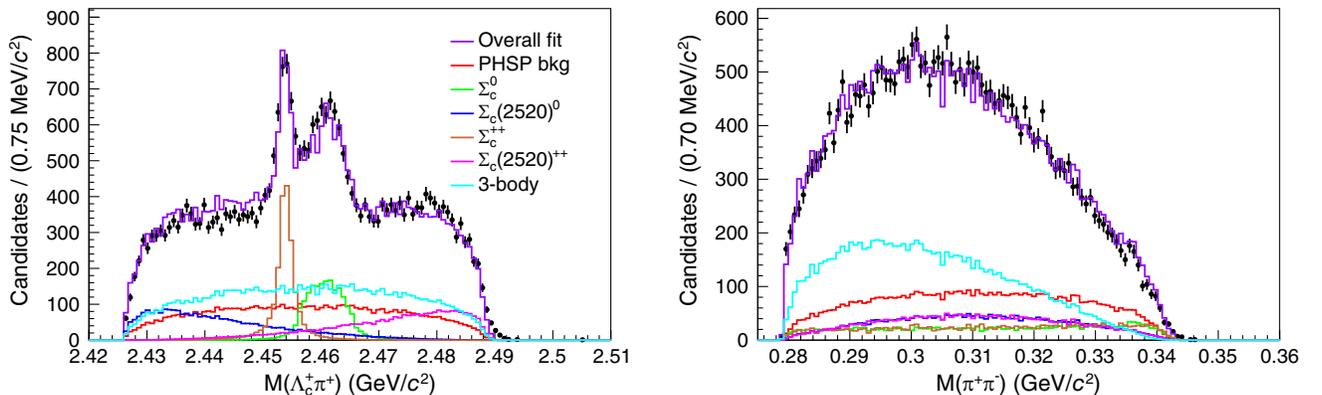
FIG. 3. Dalitz plot fit result plotted as projections. Solid lines show the overall fitted distribution and its individual components as indicated in the legend. PHSP refers to "phase space". More explanations in the text.
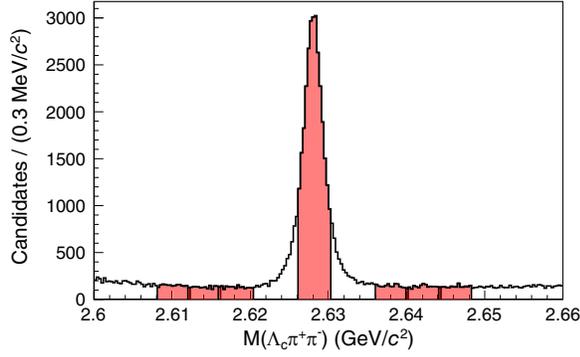
FIG. 4. Signal region and the six sideband regions on either side of the signal region used for sideband subtraction.

Figure 3 shows the projections of the fitted results with each component labeled on the plot. The Σ_c^{++} peak and the reflection peak from Σ_c^0 are evident on the $M(\Lambda_c^+\pi^+)$ mass projection. The shoulders on the left and right side of the mass region are mostly formed by the decays from the off-shell $\Sigma_c(2520)^{++/0}$. The three-body p-wave decay in the signal model shows up in the $M(\pi^+\pi^-)$ mass projection as an asymmetric distribution, in contrast to the symmetric distribution from the background phase space decay. The $\Lambda_c(2625)^+$ yield in the signal region is $N_{\text{sig}}(\Lambda_c(2625)^+) = 30319 \pm 371$. The Σ_c^0 yield is $N_{\text{sig}}(\Sigma_c^0) = 1964 \pm 66$ and the Σ_c^{++} yield is $N_{\text{sig}}(\Sigma_c^{++}) = 2022 \pm 76$. The uncertainties are statistical only.
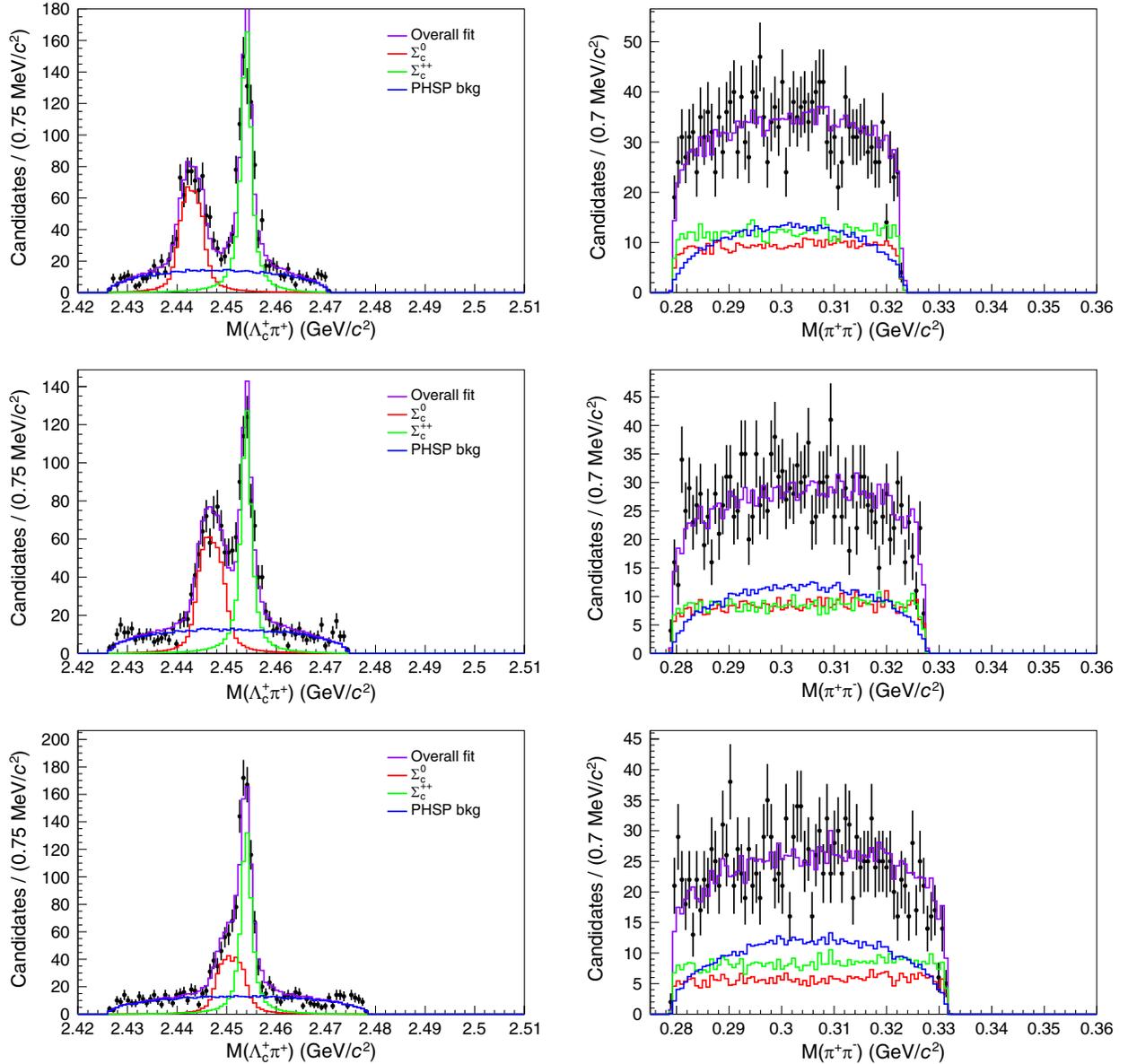
FIG. 5. Projections of the Dalitz plot fits of the three sidebands on the left side of the signal region. The overall fitted distribution and the individual fitted components are shown alongside the experimental data.
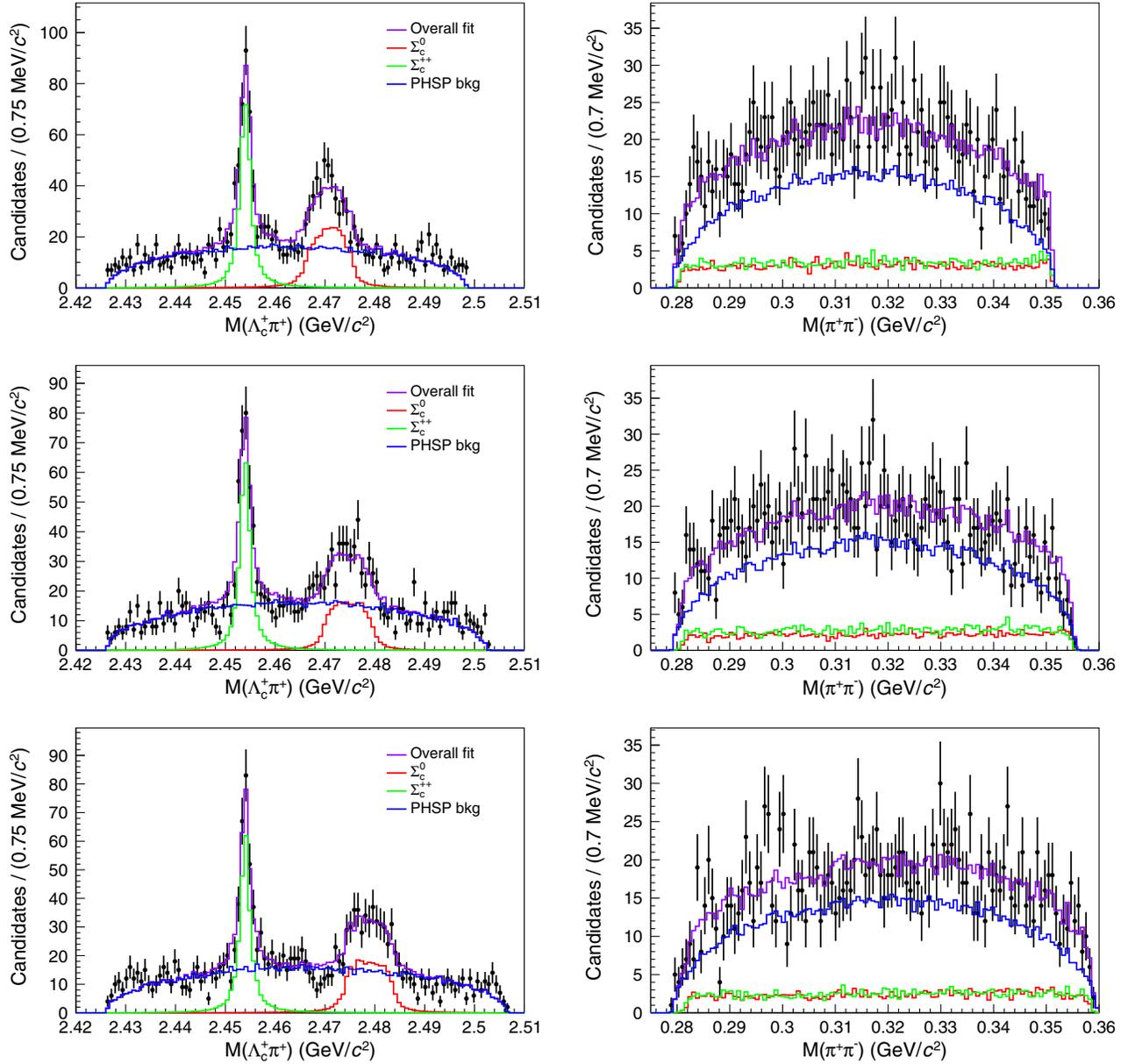
FIG. 6.   Projections of the Dalitz plot fits of the three sidebands on the right side of the signal region. The overall fitted distribution and the individual fitted components are shown alongside the experimental data.

To account for $\Sigma_c(2455)^{++/0}$ candidates that are not decay products of the $\Lambda_c(2625)^+$, the $\Sigma_c(2455)^{++/0}$ yields from the $M(\Lambda_c^+\pi^+\pi^-)$ sidebands are subtracted from the $\Sigma_c(2455)^{++/0}$ yields found from the amplitude fit. The sidebands are six 4 MeV/c^2 regions near the $\Lambda_c(2625)^+$ signal region, as shown in Fig. 4. Each sideband region is fitted as an incoherent sum of the contributions from the $\Sigma_c(2455)^0$, the $\Sigma_c(2455)^{++}$, and the three-body phase space decay. Figures 5 and 6 show the projections of the fit results for each sideband region with each component labeled on the plot. The $\Sigma_c(2455)^{++/0}$ yields in the signal region are determined by extrapolating the yields from the sidebands according to a linear fit, as shown in Fig. 7 and

tabulated in Table I. The background yields to be subtracted are $N_{\text{bkg}}(\Sigma_c^0) = 391 \pm 11$ and $N_{\text{bkg}}(\Sigma_c^{++}) = 467 \pm 12$. The branching ratio of $\Lambda_c(2625)^+ \to \Sigma_c^0\pi^+$ relative to the reference mode $\Lambda_c(2625)^+ \to \Lambda_c^+\pi^+\pi^-$ is calculated using

$$\frac{\mathcal{B}(\Lambda_c(2625)^+ \to \Sigma_c^0\pi^+)}{\mathcal{B}(\Lambda_c(2625)^+ \to \Lambda_c^+\pi^+\pi^-)} = \frac{N_{\text{sig}}(\Sigma_c^0) - N_{\text{bkg}}(\Sigma_c^0)}{N_{\text{sig}}(\Lambda_c(2625)^+)} \quad (3)$$

and similarly for the $\Sigma_c^{++}\pi^-$ mode. We note that the efficiency over the area of the Dalitz plot is found to be uniform to within the statistical precision of the MC sample simulation.
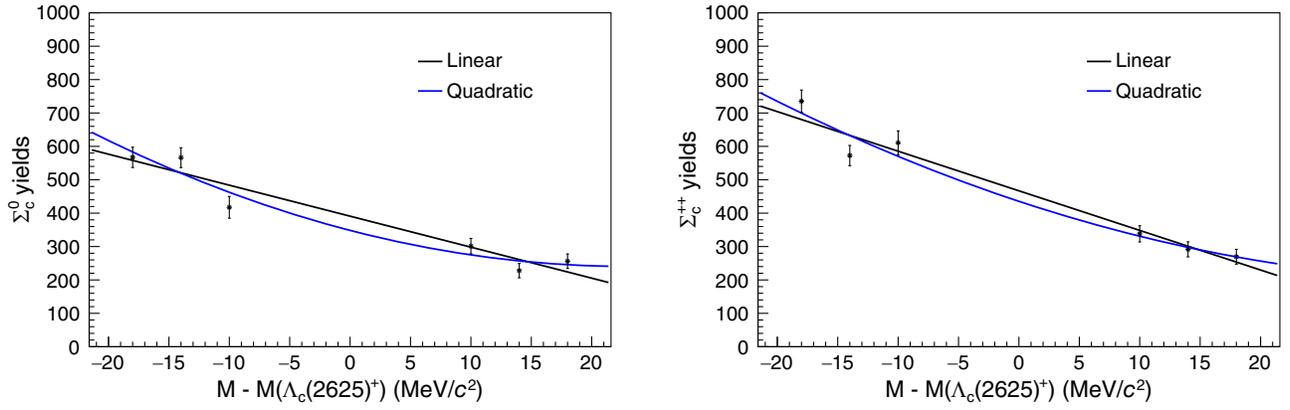
FIG. 7. Σ_c^0 and Σ_c^{++} yields from the sideband Dalitz plot fits, overlaid with linear and quadratic extrapolations.

We measure the branching ratios to be

$$\frac{\mathcal{B}(\Lambda_c(2625)^+ \to \Sigma_c^0 \pi^+)}{\mathcal{B}(\Lambda_c(2625)^+ \to \Lambda_c^+ \pi^+ \pi^-)} = (5.19 \pm 0.23)\%,$$

$$\frac{\mathcal{B}(\Lambda_c(2625)^+ \to \Sigma_c^{++} \pi^-)}{\mathcal{B}(\Lambda_c(2625)^+ \to \Lambda_c^+ \pi^+ \pi^-)} = (5.13 \pm 0.26)\%, \quad (4)$$

where the errors are statistical only.

V. SYSTEMATIC UNCERTAINTIES

The primary source of systematic uncertainty on the $\Lambda_c(2625)^+$ width is the inconsistency of the mass-resolution function between the MC sample and the experimental data. We use the $D^{*+} \to D^0 \pi^+$ decay as a control sample to determine the under- or overestimation of the mass resolution in the MC sample relative to the experimental data. The mass resolution in the experimental data is found to be 86% of that in the MC sample with track smearing, 114% without track smearing. Both mass-resolution functions are used to determine the upper limit on the $\Lambda_c(2625)^+$ width in the experimental data. When applied to the experimental data, the mass resolution without track smearing scaled by 114% results in a more conservative upper limit on the $\Lambda_c(2625)^+$ width, thus reported as the final result.

The systematic uncertainty on the $\Lambda_c(2625)^+$ mass is not greatly affected by the uncertainty on the $M(\Lambda_c^+ \pi^+ \pi^-)$ mass resolution, but is limited by the precision with which the Belle detector can measure the mass in this range. Studies with $D^{*+} \to D^0 \pi^+$ decays show that the measured

TABLE I. Subtracted yields for $\Sigma_c^{++/0}$.

Method	Σ_c^0 yield	Σ_c^{++} yield
Linear	391 ± 11	467 ± 12
Quadratic	348 ± 26	436 ± 28
Difference	11.00%	6.64%

D^{*+} mass difference with respect to the world-average value is 0.004 MeV/c^2. Any imperfection in the soft pion momentum calibration changes the measured mass of the $\Lambda_c(2625)^+$ more than that of the D^{*+}. We determine the scale factor required to correct the soft pion momentum such that the D^{*+} mass matches its PDG value, then apply the same scale factor to the daughter pions from $\Lambda_c(2625)^+$ candidates. The $\Lambda_c(2625)^+$ mass changed by 0.042 MeV/c^2, which we assign as the systematic uncertainty due to the mass scale. The track-smearing correction applied to tracks in the MC sample has a negligible effect on the mass measurement. The systematic uncertainty due to the low-momentum correction is 0.025 MeV/c^2, which is found by comparing the measured $\Lambda_c(2625)^+$ mass with and without the low-momentum correction. Summing the contributions from the mass scale and low-momentum track correction in quadrature, the total systematic uncertainty on the mass measurement is 0.049 MeV/c^2.

The systematic uncertainties on the branching ratios, which are calculated from Eq. (3), are derived from the uncertainty of the $\Lambda_c(2625)^+$ yield in the signal region, the $\Sigma_c^{++/0}$ yields fitted in the signal Dalitz plot fit, and the $\Sigma_c^{++/0}$ subtracted yields extrapolated from the sideband fits. The systematic uncertainty associated with each is tabulated in Table II. The $\Lambda_c(2625)^+$ signal yield is most affected by the mass-resolution function. We fit the experimental data with a mass-resolution function determined with and without track smearing. The difference in the yields is taken as the systematic uncertainty on the $\Lambda_c(2625)^+$ signal yield. The $\Sigma_c^{++/0}$ signal yields are determined from the Dalitz plot fit, with their masses and widths fixed to PDG values. The masses, widths, and mass resolutions are systematically varied within the PDG uncertainties, and the maximum change in the fitted $\Sigma_c^{++/0}$ yield is taken as the systematic uncertainty. In order to determine the sideband subtracted yield, the six sidebands are fitted individually to determine the $\Sigma_c^{++/0}$ yields, with the yield and uncertainty in each sideband region shown

TABLE II. The percentage systematic uncertainties of the signal yields used for the branching ratio calculation.

Source	Σ_c^0 signal (%)	Σ_c^{++} signal (%)	Σ_c^0 sideband (%)	Σ_c^{++} sideband (%)	$\Lambda_c(2625)^+$ signal (%)
Resolution	1.97	1.42	2.74	1.08	3.64
$\Sigma_c^{0/++}$ width	4.00	2.26	2.52	2.38	
$\Sigma_c^{0/++}$ mass	1.25	1.11	0.08	0.08	
Extrapolation			11.00	6.64	
MC sample size	1.91	2.09	0.71	0.22	
Total	5.01	3.57	11.63	7.14	3.64

TABLE III. Systematic uncertainties on the branching ratios.

Source	$\frac{\mathcal{B}(\Lambda_c(2625)^+\to\Sigma_c^0\pi^+)}{\mathcal{B}(\Lambda_c(2625)^+\to\Lambda_c^+\pi^+\pi^-)}$ (%)	$\frac{\mathcal{B}(\Lambda_c(2625)^+\to\Sigma_c^{++}\pi^-)}{\mathcal{B}(\Lambda_c(2625)^+\to\Lambda_c^+\pi^+\pi^-)}$ (%)
$\Sigma_c^{0/++}$ resolution	0.13	0.10
$\Sigma_c^{0/++}$ width	0.26	0.16
$\Sigma_c^{0/++}$ mass	0.08	0.07
Extrapolation	0.14	0.10
MC sample size	0.12	0.14
$\Lambda_c^+(2625)$ resolution	0.19	0.19
Total	0.40	0.32

in Fig. 7. The extrapolated yield at the nominal $\Lambda_c(2625)^+$ mass is a weighted average of the yields of the six sidebands. We take the difference between the linear and quadratic extrapolation as shown in Table I as the systematic uncertainty due to the extrapolation. To account for the statistical fluctuation due the finite MC sample sizes in the Dalitz plot fits, we compare the fitted results using two statistically independent MC samples of the same size. The difference is taken as the systematic uncertainty due to the MC sample size. With systematic uncertainties on the yields in Eq. (3) listed in Table II, the total systematic uncertainties on the branching ratios are calculated from the propagation of error and are listed in Table III. The total systematic uncertainty on the branching ratios is found to be 0.40% for the $\Sigma_c^0\pi^+$ channel and 0.32% for the $\Sigma_c^{++}\pi^-$ channel.

VI. DISCUSSION

We report the most precise $\Lambda_c(2625)^+$ mass, width, and branching ratio measurements to date. The measured mass is consistent with previous results. The measured upper limit on the $\Lambda_c(2625)^+$ width is $\Gamma(\Lambda_c(2625)^+) <$ 0.52 MeV/c^2 at the 90% confidence level. Theoretical predictions for the $\Lambda_c(2625)^+$ width vary. Arifi *et al.* predict the width to be 0.570 MeV/c^2 based on chiral and heavy quark symmetry [3]. The width is revised to be between 0.09 and 0.26 MeV/c^2 in a subsequent publication with the inclusion of relativistic corrections [5]. Kawakami and Harada predict a width in the range of 0.11–0.73 MeV/c^2 based on chiral symmetry [6]. Guo *et al.*

predict a much smaller width of 1.13×10^{-2} MeV/c^2, based on the $^3P_0$ model [7].

The branching ratios of $\Lambda_c(2625)^+ \to \Sigma_c^0\pi^+$ and $\Lambda_c(2625)^+ \to \Sigma_c^{++}\pi^-$ relative to the reference mode $\Lambda_c(2625)^+ \to \Lambda_c^{++}\pi^+\pi^-$ are extracted from a full Dalitz plot fit. Backgrounds from non-$\Lambda_c(2625)^+$ decays are subtracted from the $\Sigma_c^{++/0}$ yields. Our measurements align with the prediction by Arifi *et al.*, who assume $\Lambda_c(2625)^+$ is a λ mode excitation [3]. Kawakami and Harada predicted a wide range [6] and Guo *et al.* predicted the ratio $\Gamma(\Sigma_c^{++}\pi^-)/\Gamma_{\text{total}}$ to be 29.9% [7], which is already in contradiction with the previous measurement. Our measurements of the properties of the $\Lambda_c(2625)^+$ charmed baryon will be useful to further constrain the parameter space of the quark models and can be applied to other heavy quark systems.

VII. CONCLUSIONS

We measure the mass of the $\Lambda_c(2625)^+$ to be $2627.978 \pm 0.006 \pm 0.049$ MeV/c^2, where the uncertainty on the Λ_c^+ mass is not included since it is constrained to the PDG value during reconstruction. This is equivalent to

$$M(\Lambda_c(2625)^+) - M(\Lambda_c^+)$$
$$= 341.518 \pm 0.006 \pm 0.049 \text{ MeV}/c^2. \quad (5)$$

The mass measurement is consistent with the previous CDF measurement but with approximately half the uncertainty [2].

An upper limit on the $\Lambda_c(2625)^+$ width is determined to be

$$\Gamma(\Lambda_c(2625)^+) < 0.52 \text{ MeV}/c^2 \qquad (6)$$

at 90% confidence level which is around a factor of 2 more stringent than the previous limit.

Based on a full Dalitz plot fit and with sideband subtraction of the $\Sigma_c^{++/0}$ yields, the branching ratios relative to the mode $\Lambda_c(2625)^+ \to \Lambda_c^+ \pi^+ \pi^-$ are obtained,

$$\frac{\mathcal{B}(\Lambda_c(2625)^+ \to \Sigma_c^0 \pi^+)}{\mathcal{B}(\Lambda_c(2625)^+ \to \Lambda_c^+ \pi^+ \pi^-)} = (5.19 \pm 0.23 \pm 0.40)\%,$$

$$\frac{\mathcal{B}(\Lambda_c(2625)^+ \to \Sigma_c^{++} \pi^-)}{\mathcal{B}(\Lambda_c(2625)^+ \to \Lambda_c^+ \pi^+ \pi^-)} = (5.13 \pm 0.26 \pm 0.32)\%. \quad (7)$$

This is the first measurement made of these branching ratios, as previously only limits have been presented. These measurements can be used as inputs to theoretical models to generate predictions for other heavy quark baryons.

ACKNOWLEDGMENTS

[1] H. Albrecht *et al.* (ARGUS Collaboration), Observation of a new charmed baryon, Phys. Lett. B **317**, 227 (1993).

[2] T. Aaltonen *et al.* (CDF Collaboration), Measurements of the properties of $\Lambda_c(2595)$, $\Lambda_c(2625)$, $\Sigma_c(2455)$, and $\Sigma_c(2520)$ baryons, Phys. Rev. D **84**, 012003 (2011).

[3] A. J. Arifi, H. Nagahiro, and A. Hosaka, Three-body decay of $\Lambda_c^*(2595)$ and $\Lambda_c^*(2625)$ with the inclusion of a direct two-pion coupling, Phys. Rev. D **98**, 114007 (2018).

[4] P. A. Zyla *et al.* (Particle Data Group), Review of particle physics, Prog. Theor. Exp. Phys. **2020**, 083C01 (2020).

[5] A. J. Arifi, D. Suenaga, and A. Hosaka, Relativistic corrections to decays of heavy baryons in the quark model, Phys. Rev. D **103**, 094003 (2021).

[6] Y. Kawakami and M. Harada, Analysis of $\Lambda_c(2595)$, $\Lambda_c(2625)$, $\Lambda_b(5912)$, $\Lambda_b(5920)$ based on a chiral partner structure, Phys. Rev. D **97**, 114024 (2018).

[7] J.-J. Guo, P. Yang, and A. Zhang, Strong decays of observed Λ_c baryons in the $^3P_0$ model, Phys. Rev. D **100**, 014001 (2019).

[8] H.-Y. Cheng, Charmed baryons circa 2015, Front. Phys. (Beijing) **10**, 101406 (2015).

[9] A. Abashian *et al.* (Belle Collaboration), The Belle detector, Nucl. Instrum. Methods Phys. Res., Sect. A **479**, 117 (2002).

[10] J. Brodzicka *et al.* (Belle Collaboration), Physics achievements from the Belle experiment, Prog. Theor. Exp. Phys. **2012**, 04D001 (2012).

[11] S. Kurokawa and E. Kikutani, Overview of the KEKB accelerators, Nucl. Instrum. Methods Phys. Res., Sect. A **499**, 1 (2003).

[12] T. Abe *et al.*, Achievements of KEKB, Prog. Theor. Exp. Phys. **2013**, 03A001 (2013).

[13] D. J. Lange, The EvtGen particle decay simulation package, Nucl. Instrum. Methods Phys. Res., Sect. A **462**, 152 (2001).

[14] Reconstruction of charge conjugates is implied unless otherwise stated.

[15] R. Brun, F. Bruyant, M. Maire, A. C. McPherson, and P. Zanarini, GEANT3.21 , CERN Report No. DD/EE/84-1, 1987.

[16] M. Gelb *et al.*, B2BII: Data conversion from BELLE to BELLE II, Comput. Software Big Sci. **2**, 9 (2018).

[17] T. Kuhr, C. Pulvermacher, M. Ritter, T. Hauth, and N. Braun (Belle-II Framework Software Group), The BELLE II core software, Comput. Software Big Sci. **3**, 1 (2019).

[18] The Belle II Collaboration, Version 05-01-06 (2022), 10.5281/zenodo.6949513.

[19] E. Nakano, Belle PID, Nucl. Instrum. Methods Phys. Res., Sect. A **494**, 402 (2002).

[20] S. H. Lee *et al.* (Belle Collaboration), Measurements of the masses and widths of the $\Sigma_c(2455)^{0/++}$ and $\Sigma_c(2520)^{0/++}$ baryons, Phys. Rev. D **89**, 091102 (2014).

[21] W. Verkerke and D. P. Kirkby, The RooFit toolkit for data modeling, *eConf* C0303241, MOLT007 (2003).

[22] H. Matevosyan, R. Mitchell, and M. Shepherd, https://github.com/mashephe/AmpTools/wiki.